Soft Matter

Accepted Manuscript

ROYAL SOCIETY OF CHEMISTRY

www.rsc.org/softmatter

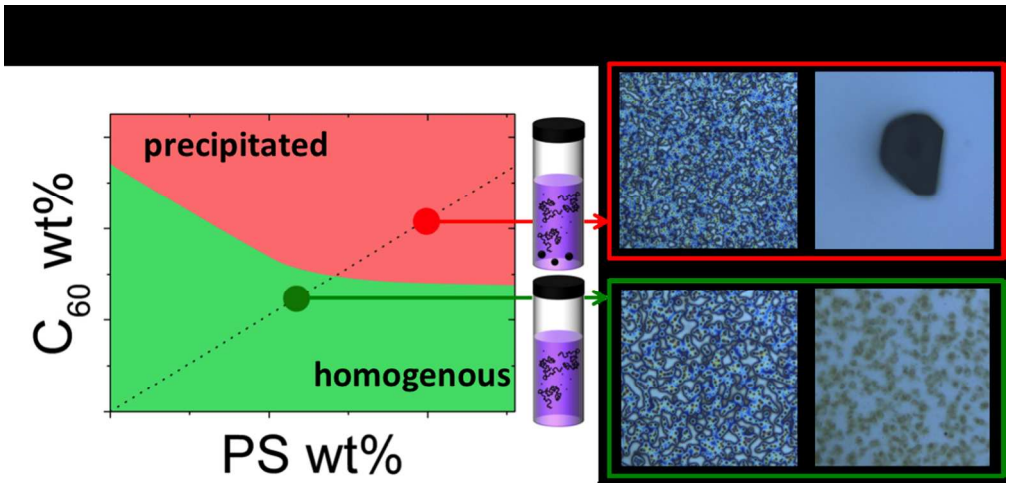

Mapping of the phase boundaries of a polymer/fullerene/solvent mixture indicates that a simple occupied chain volume argument describes the experimental data well and permits film formation, of identical composition and thickness, with well-defined morphologies.

CREATED USING THE RSC LaTeX PCCP ARTICLE TEMPLATE – SEE www.rsc.org/electronicfiles FOR DETAILS

ARTICLE TYPE www. rsc.org/xxxxxx | XXXXXXXX

Polymer fullerene solution phase behaviour and film formation pathways†

Rajeev Dattani,[a] and João T. Cabral[a]*

Received Xth XXXXXXXXXX 20XX, Accepted Xth XXXXXXXXX 20XX
First published on the web Xth XXXXXXXXXX 200X
DOI: 10.1039/b000000x

We report the phase behaviour of polymer/fullerene/solvent ternary mixtures and its consequence for the morphology of resulting composite thin films. We focus particularly on solutions of polystyrene (PS), C_{60} fullerene and toluene, which are examined by static and dynamic light scattering, and films obtained from various solution ages and thermal annealing conditions, using atomic force and light microscopies. Unexpectedly, the solution phase behaviour below the polymer overlap concentration c^* is found to be described by a simple excluded volume argument (occupied by the polymer chains) and the neat C_{60}/solvent miscibility. Scaling consistent with full exclusion is found when the miscibility of the fullerene in the solvent is much lower than that of the polymer, giving way to partial exclusion with more soluble fullerenes (phenyl-C61-butyric acid methyl ester, PCBM) and a less asymmetric solvent (chlorobenzene), employed in photovoltaics. Spun cast and drop cast films were prepared from PS/C_{60}/toluene solutions across the phase diagram to yield *identical* PS/C_{60} composition and film thickness, resulting in qualitatively different morphologies in agreement with our measured solution phase boundaries. Our findings are relevant to the solution processing of polymer/fullerene fullerene composites (including organic photovoltaics), which generally require the effective solubilisation of fullerene derivatives and polymer pairs in this concentration range, and the design of well-defined thin film morphologies.

1 Introduction

Polymer composites comprising colloids or nanoparticles (NP) are often solution processed into films, finding practical applications that range from common paints and coatings[1] to nanostructured organic electronics[2]. Polymer/fullerene/solvent mixtures are particularly significant for organic solar cells[3] and have attracted much attention as controlling thin film morphology is required to obtain high performance devices. Processing variables include film thickness, solvent or mixture of solvents, thermal and solvent annealing time/temperature, fullerene loading, polymer regioregularity and molecular weight, and are often used to empirically guide film optimisation. However, device performances of an extensively studied polymer/fullerene pair, poly(3-hexylthiophene-2,5-diyl) (P3HT) and phenyl-C61-butyric acid methyl ester (PCBM), reveal a huge disparity in the efficiency of nominally identical films.[4] While there can be various causes for such irreproducibility, two aspects of polymer/fullerene processing appear to have been largely overlooked: the phase behaviour and drying pathways of the ternary precursor solutions.

Careful studies of binary polymer/NP mixtures, typically with functionalised silica or gold NP,[6–10] have resulted in much controversy in terms of changes in polymer chain dimensions and (related) dispersion quality of the nanocomposites, which are generally cast from solution. Understanding solution miscibility, polymer conformation and NP association, and their evolution along film formation pathways is evidently required to fully exploit the potential of nanostructured composites in general.

Polymer and colloid solutions are often discussed[11] in terms of the relative dimensions of its constituents (*viz.* polymer radius of gyration R_g^{poly} and colloid R_C), defining the so-called protein ($R_C << R_g^{poly}$) and colloid ($R_C >> R_g^{poly}$) limits. Small NPs (or indeed fullerenes) may be expected to form solutions in the protein limit and cause R_g^{poly} to change, depending on

† Electronic Supplementary Information (ESI) available: [details of any supplementary information available should be included here]. See DOI: 10.1039/b000000x/

[a] *Department of Chemical Engineering, Centre for Plastic Electronics, Imperial College London, London, SW7 2AZ, United Kingdom; E-mail: j.cabral@imperial.ac.uk*

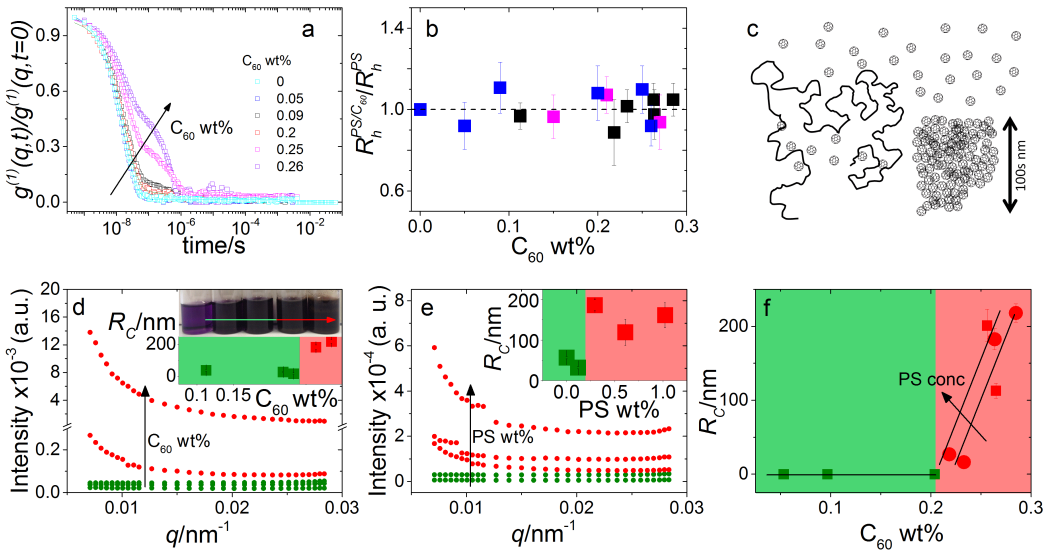

Fig. 1 (a) DLS correlation functions at 1.00±0.07 wt% PS with C_{60} from 0 to 0.26 wt%. (b) Normalised $R_h^{PS/C_{60}}/R_h^{PS}$ for 0.30±0.01 (▪), 0.6±0.1 (▪) and 1.00±0.07 wt% PS (▪). We observe no change in $R_h^{PS/C_{60}}$ with addition of C_{60}, consistent with our previous findings.[5] (c) Schematic depicting dispersed fullerenes and clusters on the order of 100s nm with unperturbed PS chains. (d-e) SLS of ternary solutions (d) increasing C_{60} concentration from 0.11 to 0.28 wt% and fixed 0.30±0.01 wt% PS and (e) increasing PS concentration from 0 to 1 wt% and fixed 0.25±0.01 wt% C_{60}. (f) Fullerene R_C is dependent on C_{60} and PS concentration, shown with 0.30±0.01 (●) and 1.00±0.07 wt% PS (▪ and ▪). Inset in (d) is an image of solution vials with increasing C_{60} loading and aggregates can be seen in the highlighted area. Inset in both (d) and (e) are estimates of C_{60} cluster sizes by a Guinier approximation.

the polymer-NP interactions in solution and their relative concentrations. Conversely, the addition of polymer can cause crystallisation of the NP, as it is found in protein solutions and from which the term 'protein limit' is derived[12]. Solutions in the colloid limit can be expected for large colloids but also for clusters, for instance of poorly-dispersed NPs. Dispersed fullerenes have $R_C \approx 0.5$ nm which, for most polymer masses M_W (including those considered in this work), should result in solutions in the protein limit. Theoretically, multiple interactions between each polymer coil and colloidal particles must thus be considered, and polymers are generally treated as chains of connected spheres, each of the size of a colloidal particle. Both homogenous[13,14] and phase separated[15–17] solutions have been predicted theoretically. Experimentally, phase separation and crystallisation has been observed in a number of systems[5,18–21]. In all cases, the polymer was a linear polystyrene chain and the small colloid was either octa-n-propylsilsesquioxane (R_C = 0.7 nm), crosslinked poly (ethyl methacrylate) (R_C = 8-42 nm), hydroxyl functionalized silica nanoparticles (R_C = 11 nm) or C_{60} fullerene (R_C = 0.35 nm). For some systems, significant coil contraction (≈ 50%) was found in the presence of high enough (≳ 8 wt%) colloid concentration.[18–21]

In this work, we examine polymer/fullerene/solvent mixtures by comprehensively characterising the ternary solution phase behaviour and resulting (binary) polymer/fullerene film morphologies. We select polystyrene (PS) as the polymer matrix, fullerene C_{60}, and toluene as a model system; while PS is fully miscible in toluene across the entire composition range, the reported miscibility of C_{60} in toluene is only 0.32 wt%[22]. The miscibility of C_{60} is PS is estimated to be 1 wt% or lower[23], although higher 'dispersibility' limits are found for rapidly precipitated[23,24] or spin cast composite films[25,26]. This PS/C_{60}/toluene system exhibits therefore highly asymmetric solvent interactions, in that the solubility of the PS is much greater

than that of C_{60} in toluene. For comparison, in order to decrease asymmetry in solubility, we also evaluate solutions comprising a more miscible fullerene, phenyl-C61-butyric acid methyl ester (PCBM), in toluene, and a solvent exhibiting considerably higher PCBM solubility, chlorobenzene.

Previous studies on annealed binary PS/C_{60} thin films have shown a rich morphological behaviour, ranging from (meta)stable to rapidly dewetting films, from homogeneous and uniform to phase separated (sparsely nucleated to spinodally correlated) morphologies, and various coupling effects between these.[25–31] Under certain conditions, an enriched C_{60} layer was reported at the substrate interface[25,27,28], albeit not generally[30]. Morphological control parameters were found to include the polymer mass M_W[26], fullerene content[29], substrate surface energy[25,30,31], film thickness, temperature, and even light exposure (due to fullerene photo-chemistry in both films[30] and solutions[32]).

We now seek to measure the solution phase behaviour and quantify its impact on the film morphology, in both as-cast and thermally annealed films. Our hypothesis is that films of *identical* composition and thickness can exhibit considerable morphological differences arising from both their initial solution state and film formation pathway. We therefore evaluate R_C and R_g^{poly} in solution by static (SLS) and dynamic light scattering (DLS) to gauge miscibility, and film morphology by optical (OM) and atomic force microscopies (AFM) to correlate, for the first time, the solution and film properties of these academically and technologically important polymer-fullerene mixtures.

2 Experimental

Fullerene C_{60} (99%+ purity) was purchased from MER Corp, polystyrene of molecular mass (M_W) 65 kg/mol and polydispersity index 1.1 from Polymer Laboratories Ltd (referred to as 65k), and toluene (99.5% purity) from VWR. The necessary masses of C_{60} and PS were weighed into the same vial and the required mass of toluene added. The resulting PS/C_{60}/toluene solutions were stored in the dark (as light exposure is known to cause fullerene aggregation[32]) and stirred for 48 hours. All solution concentrations can be found in Table S1†. Details of additional systems investigated, namely PS M_W from 18 to 775 kg/mol, as well as PCBM fullerene and cholorobenzene solutions are provided in Supporting Information.

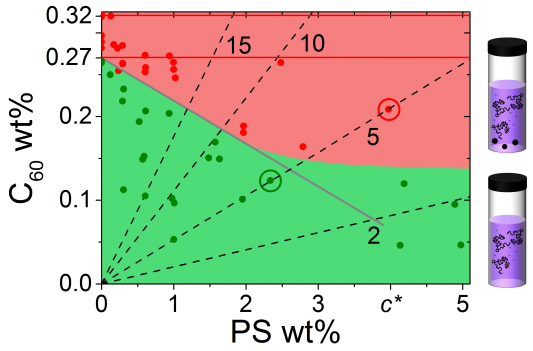

Fig. 2 Phase diagram of PS/C_{60}/toluene solutions showing C_{60} aggregation at 0-5 wt% PS. Homogenous (•) and precipitated (•) solutions are shown. The calculated solubility limit (—) (described in the text) agrees well with the observed homogenous and precipitated phases, shown in green and red respectively. Red lines indicate neat C_{60}/toluene miscibility, previously reported (0.32 wt%)[22] and found in this study (0.27 wt%). Dashed lines indicate constant PS/C_{60} ratio in the film, with the C_{60} mass % noted. The circled data points, along the PS-5wt% C_{60} line, indicate solutions employed in thin films investigated below.

For static light scattering (SLS) a SOFICA instrument (Societé Francaise d'Instruments de Contröle et d'Analyses, Le Mesnil Saint-Denis, S. et 0., France), modified by SLS Systemtechnik (G. Baur, Denzlingen, Germany) was employed. The SLS is equipped with a 5 mW HeNe laser source (λ =633 nm) and a goniometer covering $27 \leq \theta \leq 105°$, and yielding a wavenumber range from $7.1 \leq q \leq 23.7 \times 10^{-3}$ nm^{-1}, calculated using $q = \frac{4\pi n}{\lambda} \sin\frac{\theta}{2}$, where n is the refractive index of the solvent. Experiments were carried out on 2 mL of solution in cylindrical quartz cells with 1 cm diameter (Hellma, Müllheim, Germany) and a stopper to prevent evaporation. The light exposure during SLS measurement was kept below 3-5 minutes to minimise photo-oxidation of fullerenes. The photomultiplier was calibrated with a toluene (puriss. p.a. ≥ 99.7%, Sigma Aldrich) standard. SLS data was treated with the standard Guinier approximation to obtain R_C:

$$\ln R(q) = \ln R_0 - \frac{q^2 R_C^2}{3} \quad (1)$$

Dynamic light scattering (DLS) experiments were carried out with a Malvern Nano-S (Malvern Instruments Ltd, UK) with a fixed detector at 173°, corresponding to $q = 2.96 \times 10^{-2}$ nm^{-1}. All experiments

were performed in sealed, rectangular quartz cuvettes (Hellma, Müllheim, Germany). To account for the multiple decays correlation functions were fit using a sum of exponential decays:

$$g^{(1)}(q,t) = \sum_{i=1}^{N} a_i(q)\exp(-\Gamma_i(q)t) \qquad (2)$$

where $1 \leq i \leq 3$, and $\Gamma_i = D_i q^2$ from which the diffusion coefficient for the i^{th} mode, D_i, can be found. Using $R_{h,i} = \frac{k_B T}{6\pi\eta D_i}$, where k_B, T and η are Boltzmann's constant, temperature (K) and the viscosity of the solvent respectively, the hydrodynamic radius of the i^{th} mode, $R_{h,i}$, can be found.

Thin films were fabricated from the appropriate solution via spin coating onto 1 cm^2 <100> silicon substrates (Compart Tech) which were surface treated with a Ultraviolet UV Ozone Cleaner (Novascan) for 15 minutes. The spin coating frequency (rpm) was varied as necessary in order to achieve the *same* film thickness from solutions of different PS concentrations (thickness calibration is shown in Figure S2†). Prior to measurement, film thicknesses were measured with a UV-visible interferometer (Filmetrics, F20-UV) calibrated with a SiO_2 wafer standard. All films obtained via spin casting reported here are 130±3 nm thick. Drop cast samples were prepared by casting 50-100μL of solution (the higher PS concentration solutions were cast with a lower volume to maintain identical film thickness) onto 1 cm^2 Si substrates at 60 °C and dried for 30 minutes resulting in thicknesses of ≈20 μm.

Polymer/fullerene composite films were first imaged with an Olympus BX41M-LED reflectance microscope equipped with a AVT GigE GX1050C camera. Image analysis was carried out using ImageJ (v1.46r). Brightness and condenser/focussing settings were varied for maximum contrast between polymer-rich and fullerene-rich regions, intensity thresholded and a fast Fourier transform and/or particle analysis was carried out. Atomic force microscopy (AFM) (Innova, Bruker) is employed in tapping mode to quantify nanoscale structures and topography in thin polymer composite films. Image files were processed using Gwyddion (v2.31): the raw AFM data was imported, levelled by mean plane subtraction, a polynomial background removed and lines corrected by matching height median; the minimum height for all images was set to zero.

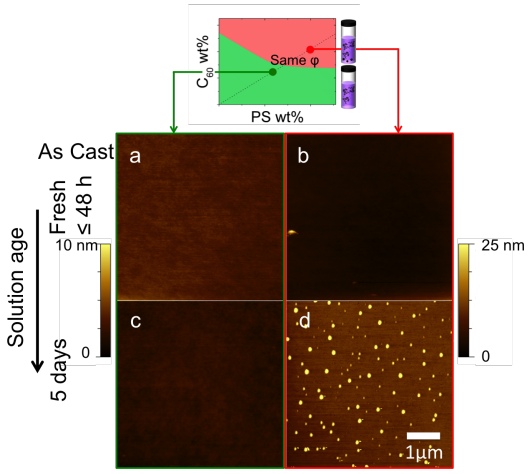

Fig. 3 Effect of solution age on spun cast thin films, across the miscibility boundary. AFM topography images of 5% C_{60}/PS 130 nm as-cast thin films prepared from (a-b) a freshly made solution and (c-d) a solution aged for 5 days.

3 Results and Discussion

Previously, using DLS, SLS and small angle neutron scattering (SANS), we have demonstrated that PS chain dimensions remain unperturbed across the dilute to semi-dilute regimes (0 to 9.5 wt% PS) with C_{60} concentrations ranging from 0 to 0.96 wt% and a molecular weight range of 20 to 1000 kg/mol.[5] Specifically we have quantified the hydrodynamic radius R_h^{poly} obtained from DLS and the radius of gyration R_g^{poly} obtained by SLS and SANS in the dilute regime, as well as the correlation length ξ obtained by SANS in semi-dilute solutions. The experimental results for this system are consistent our previous findings. Figure 1a shows DLS correlation functions obtained at constant polymer concentration and increasing C_{60} loading. The first decay in $g^{(1)}(q,t)$ corresponds to the polymer coil whose dimensions are shown to remain unchanged across the composition range in Figure 1b. However, an additional decay appears with increasing C_{60} loadings in Figure 1a which we have found to correspond to fullerene clusters.[5]

SLS was used to probe C_{60} cluster formation by polymer addition in solution and thus gauge solution miscibility. We first measured the exact fullerene solubility limit for our C_{60} grade in toluene by stirring solutions of various concentrations for 48h, in the absence of light, at room temperature. We find a misci-

bility limit of 0.27 wt% C_{60} in toluene, below the 0.32 wt% reported previously.[22] This difference may be due to the purity of the fullerene of solvents employed, but also possibly measurement method and aggregation kinetics. We note that Ref. 22 measured solubility by dilution and filtration of a saturated C_{60} solution, while we have prepared fresh solutions at each composition which we have found to be more reproducible.

Typical SLS datasets are shown in Figure 1d and e from which the fullerene cluster size dependence with C_{60} (Fig. 1d) and PS (Fig. 1e) concentration is estimated. We find that increasing either eventually leads to C_{60} clustering beyond a composition-specific threshold; for instance, increasing PS loading causes C_{60} cluster formation at lower C_{60} concentrations, as shown in Figure 1f. At sufficiently long times and/or concentrations, macroscopic C_{60} become visible to the naked eye. A schematic illustrating these findings is shown in Figure 1c.

We next map the phase diagram by measuring a wide range of (C_{60},PS) concentrations in the dilute and semi-dilute regime of 65k PS, shown in Figure 2. The green and red points and shaded areas define the miscible and two-phase regimes. We find that the addition of PS decreases C_{60} miscibility in a *linear* fashion, until a PS concentration ($< c^*$) beyond which it becomes largely insensitive to further polymer addition. The initial linear decrease with polymer concentration suggests an expulsion of the fullerenes from the volume occupied by the PS chains, effectively increasing the fullerene concentration in a reduced available volume.

Given the (finite) miscibility of fullerenes in polystyrene, one could expect that the addition of a sufficiently small polymer fraction would not appreciably alter C_{60} miscibility in the ternary solution. This is not observed experimentally and, instead, the C_{60} miscibility drops from the outset of PS addition. In order to rationalise these findings we consider the simplest possible scenario: that the C_{60} miscible fraction in solution is set by the volume remaining, V_{free}, after subtracting the volume occupied by the polymer chains, V_{occ}, from the total solution volume, V_{total}, yielding

$$V_{free} = V_{total} - \alpha\left(N\frac{4\pi R_g^3}{3}\right) \qquad (3)$$

where V_{occ} is computed as $\left(N4\pi R_g^3/3\right)$ where N is the number density of chains (proportional to concentration) and the dilute solution $R_g(PS)$ is calculated by $R_g(\text{nm})=1.25\times10^{-5}M_W^{0.595}$ in toluene.[33] Effectively, the

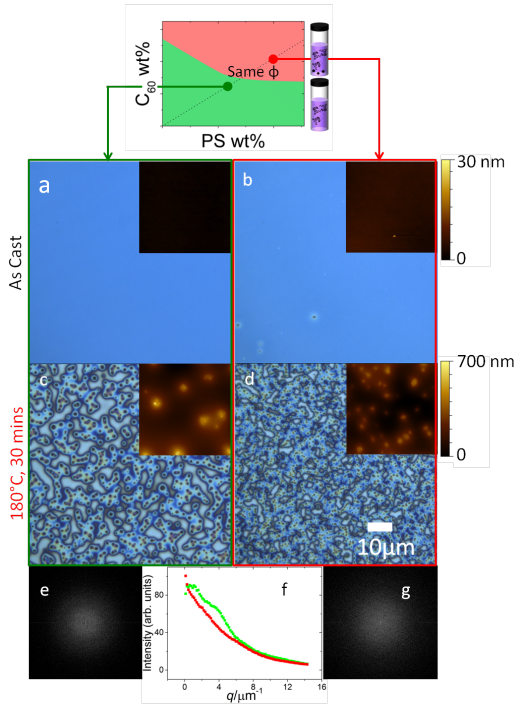

Fig. 4 Effect of thermal annealing (180 °C, 30 min) on the morphology of spun cast 5% C_{60}/PS 130 nm thin films prepared from solutions in the (a,c) homogenous and (b,d) precipitated regimes. Although the (a,b) as-cast thin films and (c,d) after annealing. FFTs of (c) and (d) are shown in (e) and (g) respectively, whose radial profiles are compared in (f). Insets in (a-d) show AFM scans of the corresponding films, with image width of 10 μm; the height scale bars are 30 nm in (a-b) and 700 nm in (c-d).

fullerene concentration is assumed to increase in the remaining V_{free} and we take the miscibility of C_{60} in toluene to remain unchanged. The scaling pre-factor α sets the gradient of the line shown in grey in Figure 2. We obtain a best fit for $\alpha = 0.74$. Incidentally, we note that this value corresponds to the close packing of equal (impenetrable) spheres. Broadly speaking, the various estimates for c^*, rest on similar volume estimates[34,35] of single chain overlap and agreement with experimental data is often not quantitative,[36] as the semi-dilute crossover is broad. Beyond $\sim\frac{2}{3}c^*$ the concentration of molecularly dispersed C_{60} appears to level off to value between 0.12 and 0.15 wt%. This result agrees with previous estimates of finite miscibility of C_{60} in polystyrene[23,24] which we have estimated to be <1 wt% C_{60}.[23] As expected, at sufficiently

high polymer concentration, when chain overlap begins, fullerene miscibility no longer correlates with the simple volume estimate extrapolated from dilute chain dimensions. The asymptotic fullerene miscibility value should now be governed by binary thermodynamic interaction with the host polymer matrix.

Given the strong powerlaw dependence of the volume occupied by single chains (and c^*) on polymer mass M_W, we have carried out selected experiments by varying PS M_W (presented in Figure S1†). As expected from eq. 3, increasing M_W decreases c^* and the miscibility of C_{60} decreases at a faster rate by addition of PS, as chains overlap 'earlier' (i.e. at a lower concentration). The slope α remained consistent with the value found above. We are thus surprised that this simple scaling model yields remarkable agreement with our data.

We can thus summarise our findings for PS/C_{60}/toluene ternary solutions as follows: (i) increasing PS wt% increases C_{60} aggregate size (at constant solution age); (ii) the onset of C_{60} aggregation depends on PS concentration with higher PS loadings inducing C_{60} aggregation at lower C_{60} concentrations; (iii) at a fixed mass, increasing the M_W of PS chains decreases the miscibility limit of C_{60}; (iv) a simple volume argument below c^* describes the trend observed for the miscibility of C_{60} by polymer addition of various M_W.

We next consider the effect of ternary solution behaviour on the resulting PS/C_{60} film morphology, both for thin and bulk films, both as-cast and thermally annealed. While increasing polymer content generally increases film thickness obtained by spin coating, carefully coupling rpm and PS concentration allows films of identical thickness to be prepared from solutions with a range of solids content. Our calibration curve for PS/C_{60}/toluene is shown in Figure S2†. Maintaining the PS to C_{60} ratio constant, indicated by the dashed lines in Figure 2, nominally *identical* films can be prepared. Illustrative 5% C_{60}/PS films, on both sides of the miscibility boundary, are indicated by red and green circles in Figure 2. We investigate the effects of solution age, thermal annealing and drying time.

3.1 Solution Age

Over time, C_{60} within solutions in the precipitated regime (red) is found to aggregate. Figure 3 compares the morphology of films which are nominally identical: 5% C_{60}/PS and 130 nm thick. Films cast from the immiscible (red) region yield C_{60} clusters whose number (density) increases with solution age (up to 5 days shown here). By contrast, films cast from the miscible (green) region yield uniform films regardless of solution age. This behaviour was confirmed along other fixed relative C_{60}/PS composition lines (e.g. Figure S3†).

3.2 Thermal Annealing

Annealing of thin films prepared from the two solution states, across the phase boundaries, yielded strikingly different morphologies shown in Figure 4. Since the miscibility of C_{60} in PS is relatively low (<1% mass[23]), one expects films cast for solutions with a higher C_{60} content to yield phase segregated morphologies[29] upon thermal annealing above the glass transition temperature T_g of the mixtures (between 104-108 °C[23]). As seen previously (Fig 3a,b), as-cast film prepared from homogenous solutions (green) are uniform, whereas those from precipitated solutions (red) exhibit micron sized aggregates. Upon annealing, a characteristic 'spinodal clustering'[26,29] morphology can be observed in the film prepared from the homogenous solution (Figure 4c), whereas the annealed morphology of films prepared from the precipitated solution is markedly different, exhibiting more and, on average, smaller C_{60} clusters. The seed clusters from solution appear thus to alter the fullerene cluster formation in films, which seems dominated by fast nucleation (in addition to growth of seed clusters). Representative fast Fourier transforms (FFTs) show that the dominant lengthscale of films cast from homogeneous solutions (seen by a shoulder in the structure factor, green) is lost due to the polydisperse morphology of films cast from metastable solutions (in red).

3.3 Drying timescales and film thickness

We next consider the effect of film casting method on the resulting film morphology. Given that the drying timescale of spin coating is relatively short (a few seconds), the 'as-cast' films obtained are found to quench morphologies closely matching the expectations from the solution state. As such, films spun cast from the miscible region of the solution phase diagram appear homogenous, even though their composition exceeds the miscibility limit of C_{60} in PS melts, since below T_g. By contrast, films drop cast from solution may take up to 30 min to dry (above room temperature) and will

thus explore the same drying pathway, across the miscibility limit, at a much slower rate. Drop casting from heterogeneous (red) solutions, should thus differ from spin casting, by allowing a slow crossing of the phase boundaries in addition to the growth of seed C_{60} clusters. The common drying pathway is shown in Figure 5 and maintains a constant PS to C_{60} ratio throughout, and thus yields identical film compositions (and thickness through judicious choice of casting parameters).

The slower drop casting yields dramatically different composite morphologies, shown in Figures 5e-h. Films cast from the homogeneous (green) solutions yield few ~ 1 μm clusters, as seen by optical microscopy in Figure 5e, that nucleated during drying through the heterogeneous pathway. Upon thermal annealing above T_g, diffuse C_{60} clusters of several μm form (Figure 5g), with a structure reminiscent of bundles with a ramified internal structure. Large (~100 μm) fractal fullerite C_{60} structures from toluene can be obtained under specific slow evaporation conditions,[37] suggesting that the slow evaporation and higher viscosity of PS/toluene drop casted solutions yields these 'tumbleweed' structures. Directional assembly of C_{60} in solution with rod-like (and other) features,[38,39] and for polymer/colloid mixtures[40] have been observed previously. By contrast, films drop cast from aggregated solutions (red) yield large (10s μm) C_{60} compact crystalline (and birefringent) clusters regardless of annealing, as shown in Figures 5f and h (and S4†), suggesting that solution seed clusters grow extensively during the slow drying period and thus thermal annealing has no incremental (nucleation and growth) effect. The controlled growth of C_{60} micron-sized crystals with various shapes and crystal structures using solvent mixtures has been demonstrated (e.g. Ref. 41). The drying pathway, across both sides of the phase boundary, has evidently a significant impact and potential in tuning the morphology of these polymer/fullerene composites.

4 Conclusions

We examined the ternary solution phase behaviour of a model PS/C_{60}/toluene mixture to elucidate the effect of the addition of a polymer to the miscibility of C_{60}, as well as the effect of C_{60} on the polymer conformation. As we have shown previously[5] and corroborated with this work, the conformation of PS remains unperturbed across the dilute and semi-dilute regimes. By contrast, the addition of PS to C_{60}/toluene solutions linearly decreases the miscibility limit of C_{60} in the mixture compared to that in neat toluene. We find that a simple volume argument assuming that the C_{60} concentration effectively increases by subtraction of the volume occupied by single PS chains describes remarkably well the experimental observations below c^* for several M_W. We find that the C_{60} miscibility eventually becomes largely insensitive to further PS addition between 0.12 and 0.15 wt% C_{60}, which is compatible with the estimate of <1% wt for PS/C_{60} (binary) mixtures.[23]

To assess the generality of our findings, we examined PS/toluene solutions with a more soluble fullerene (PCBM), and PS/PCBM solutions with a better solvent for the fullerene: chlorobenzene. These results are summarised in Figures S5 and S6†. In short, we find that the phase boundaries vary qualitatively in a similar manner, i.e. a linear decrease in fullerene miscibility upon polymer addition. However, the volume estimate with $\alpha \simeq 0.74$ (reminiscent of hard sphere packing) only applied to PS/C_{60}/toluene which we attribute to the large asymmetry in the solubility of PS and C_{60} in toluene. As this asymmetry decreases (e.g. with PCBM and further with chlorobenzene), the miscibility reduction becomes less sensitive to polymer addition, effectively reducing α (all the way to $\simeq 0$). Fullerene miscibility and aggregation appears thus highly dependent on the *relative* magnitude of the interactions between the solution components.

We have considered PS/C_{60} film morphologies obtained for *identical* compositions and thicknesses but formed through different solution pathways. In agreement with the measured phase diagram, we observe films that are rapidly formed by spin casting from the homogeneous region to be uniform, while those cast from above the miscibility line to contain clusters, that depend on solution age. Upon thermal annealing, these also yield different morphologies indicating opportunities for tuning film morphology by controlling the solution properties, which have not been previously recognised. Slow drying of thick (>μm) films by drop casting has a proportionally larger effect on the resulting morphology (of nominally identical films) by increasing the timescale for fullerene aggregation across the phase boundaries.

Our findings highlight the importance of understanding solution properties of polymer/fullerene (and polymer/nanoparticle) composites in a range of practical applications, including fullerene-based solar cells and advanced coatings that are solution processed.

5 Acknowledgements

The authors thank the Engineering and Physical Sciences Research Council (EPSRC) for funding (EP/G037515/1), the Royal Society (UK) for an International Exchange award, and the Institute for Molecular Engineering (IME) at the University of Chicago for generous hospitality of JTC. We thank Klaus Huber (Universität Paderborn, Germany) and Jack Douglas (NIST, Maryland) for many thought provoking and useful discussions.

References

1 J. Keddie and A. F. Routh, Fundamentals of Latex Film Formation - Processes and Properties, Springer Laboratory, 2010.
2 J. Rivney, S. C. B. Mannsfeld, C. E. Miller, A. Salleo and M. F. Toney, Chemical Reviews, 2012, 5488–5519.
3 B. C. Thompson and J. M. J. Fréchet, Angewandte Chemie (International ed. in English), 2008, **47**, 58–77.
4 M. T. Dang, L. Hirsch and G. Wantz, Advanced Materials, 2011, **23**, 3597–3602.
5 R. Dattani, R. Michels, A. J. Nedoma, R. Schweins, P. Westacott, K. Huber and J. T. Cabral, Macromolecules, 2014, **47**, 6113–6120.
6 A. I. Nakatani, W. Chen, R. G. Schmidt, G. V. Gordon and C. C. Han, Polymer, 2001, **42**, 3713–3722.
7 S. Sen, Y. Xie, S. Kumar, H. Yang, A. Bansal, D. Ho, L. Hall, J. Hooper and K. Schweizer, Physical Review Letters, 2007, **98**, 128302.
8 A. Tuteja, P. M. Duxbury and M. E. Mackay, Physical Review Letters, 2008, **100**, 77801.
9 N. Jouault, F. Dalmas, S. Said, E. Di Cola, R. Schweins, J. Jestin and F. Boué, Macromolecules, 2010, **43**, 9881–9891.
10 M. K. Crawford, R. J. Smalley, G. Cohen, B. Hogan, B. Wood, S. K. Kumar, Y. B. Melnichenko, L. He, W. Guise and B. Hammouda, Physical Review Letters, 2013, **110**, 196001.
11 K. J. Mutch, J. S. van Duijneveldt and J. Eastoe, Soft Matter, 2007, **3**, 155–167.
12 A. Polson, G. Potgieter, J. Largier, G. Mears and F. Joubert, Biochimica et Biophysica Acta, 1964, **82**, 463–475.
13 T. Odijk, Macromolecules, 1996, **29**, 1842–1843.
14 P. G. de Gennes, Comptes Rendus de l'Académie des Sciences, 1979, **288**, 359–361.
15 R. Sear, Physical Review E, 1998, **58**, 724–728.
16 R. Sear, Physical Review Letters, 2001, **86**, 4696–4699.
17 P. V. D. Schoot, Macromolecules, 1998, **31**, 4635–4638.
18 T. Kramer, S. Scholz, M. Maskos and K. Huber, Journal of Colloid and Interface Science, 2004, **279**, 447–57.
19 T. Kramer, R. Schweins and K. Huber, Macromolecules, 2005, **38**, 151–159.
20 T. Kramer, R. Schweins and K. Huber, Macromolecules, 2005, **38**, 9783–9793.
21 T. Kramer, R. Schweins and K. Huber, The Journal of Chemical Physics, 2005, **123**, 014903.
22 R. S. Ruoff, D. S. Tse, R. Malhotra and D. C. Lorents, J Phys Chem, 1993, **97**, 3379–3383.
23 H. C. Wong, A. Sanz, J. F. Douglas and J. T. Cabral, Journal of Molecular Liquids, 2010, **153**, 79–87.
24 M. E. Mackay, A. Tuteja, P. M. Duxbury, C. J. Hawker, B. Van Horn, Z. Guan, G. Chen and R. S. Krishnan, Science, 2006, **311**, 1740–1743.
25 K. A. Barnes, J. F. Douglas, D.-W. Liu and A. Karim, Advances in Colloid and Interface Science, 2001, **94**, 83–104.
26 H. C. Wong and J. T. Cabral, Physical Review Letters, 2010, **105**, 38301.
27 M. Holmes, M. Mackay and R. Giunta, Journal of Nanoparticle Research, 2007, **9**, 753–763.
28 M. A. Yaklin, P. M. Duxbury and M. E. Mackay, Soft Matter, 2008, **4**, 2441–2447.
29 H. C. Wong and J. T. Cabral, Macromolecules, 2011, **44**, 4530–4537.
30 H. C. Wong, A. M. Higgins, A. R. Wildes, J. F. Douglas and J. T. Cabral, Advanced Materials, 2012, **25**, 985–991.
31 S. Roy, D. Bandyopadhyay, A. Karim and R. Mukherjee, Macromolecules, 2015, **48**, 373–382.
32 R. Dattani, K. F. Gibson, S. Few, A. J. Borg, P. A. DiMaggio, J. Nelson, S. G. Kazarian and J. T. Cabral, Journal of Colloid and Interface Science, 2015, **446**, 24–30.
33 K. Huber, S. Bantle, P. Lutz and W. Burchard, Macromolecules, 1985, **18**, 1461–1467.
34 M. Daoud, J. P. Cotton, B. Farnoux, G. Jannink, G. Sarma, H. Benoit, C. Duplessix, C. Picot and P. G. de Gennes, Macromolecules, 1975, **8**, 804–818.
35 J. P. Cotton, M. Nierlich, F. Boue, M. Daoud, B. Farnoux, G. Jannink, R. Duplessix and C. J. Picot, The Journal of Chemical Physics, 1976, **65**, 1101–1108.
36 Q. Ying and B. Chu, Macromolecules, 1987, **20**, 362–366.
37 I. Zolotukhin, L. Yanchenko and E. Belonogov, JETP Letters, 1998, **67**, 720–722.
38 V. Georgakilas, F. Pellarini, M. Prato, D. M. Guldi, M. Melle-Franco and F. Zerbetto, Proceedings of the National Academy of Sciences of the United States of America, 2002, **99**, 5075–80.
39 C. Park, H. J. Song and H. C. Choi, Chemical communications (Cambridge, England), 2009, 4803–5.
40 V. J. Anderson and H. N. W. Lekkerkerker, Nature, 2002, **416**, 811–5.
41 J. Jeong, W.-S. Kim, S.-I. Park, T.-S. Yoon and B. H. Chung, The Journal of Physical Chemistry C, 2010, **114**, 12976–12981.

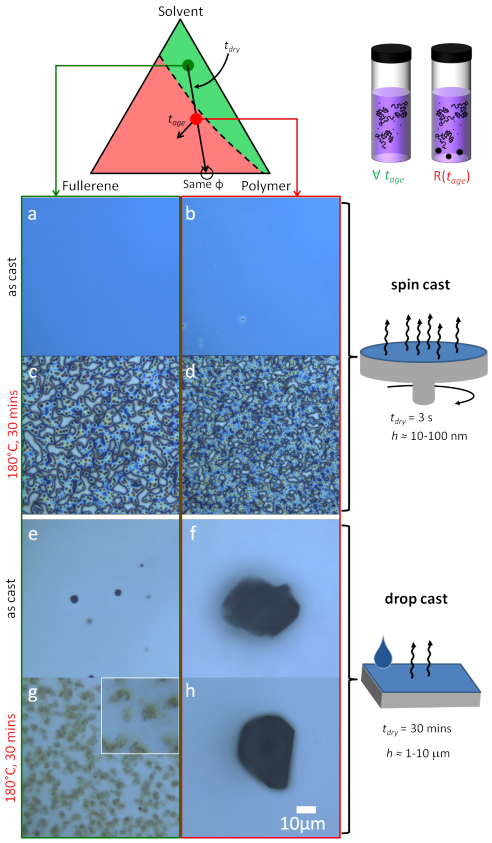

Fig. 5 Effect of drying time along the same film formation pathway. (a-d) 5 wt% C_{60}/PS 130 nm thin films fabricated via spin casting yield either an ordered (c) or disordered (d) morphology upon annealing. (e-h) 5 wt% C_{60}/PS ≈ 20 μm thick drop cast films result in (e) spare fullerene clusters nucleated during drying from homogenous solutions (green), or (f) large precipitates seeded within the precipitated solution (red) that grow during slow drying. Upon thermal annealing, (g) clusters with a ramified internal structure form from homogenous solutions and (h) large clusters, similar to those of as-cast films from the precipitated solution. Image width of inset in (g) is 10 μm. Image analysis is shown in Figure S4†.